

## Spectral Dynamics in Broadband Frequency Combs with Overlapping Harmonics

Weichen Fan<sup>1</sup>, Furkan Ayhan<sup>2</sup>, Thibault Wildi<sup>1</sup>, Mikhail Volkov<sup>3</sup>, Ali Seer,<sup>3</sup> Markus Ludwig<sup>1,†</sup>, Thibault Voumard<sup>1,‡</sup>, Andreas Brodschelm<sup>1,§</sup>, Victor Brasch<sup>4</sup>, Luis Guillermo Villanueva,<sup>2</sup> and Tobias Herr<sup>1,5,\*</sup>

<sup>1</sup>Deutsches Elektronen-Synchrotron DESY, Notkestraße 85, 22607 Hamburg, Germany

<sup>2</sup>École Polytechnique Fédérale de Lausanne, 1015 Lausanne, Switzerland

<sup>3</sup>TOPTICA Photonics, 82166 Graefelfing, Munich, Germany

<sup>4</sup>Q.ANT GmbH, Handwerkstraße 29, 70565 Stuttgart, Germany

<sup>5</sup>University of Hamburg, Luruper Chaussee 149, 22607 Hamburg, Germany



(Received 10 March 2025; accepted 29 September 2025; published 21 November 2025)

Optical frequency combs and their spectra of evenly spaced discrete laser lines are essential to modern time and frequency metrology. Recent advances in integrated photonic waveguides enable efficient nonlinear broadening of an initially narrowband frequency comb to multi-octave bandwidth. Here, we study the nonlinear dynamics in the generation of such ultrabroadband spectra where different harmonics of the comb can overlap. We show that a set of interleaved combs with different offset frequencies extending across the entire spectrum can emerge, which can be arranged into a practically evenly spaced ultrabroadband frequency comb when the initial comb is offset-free.

DOI: 10.1103/kgd7-52hy

Optical frequency combs and their discrete spectra enable phase-coherent links across the electromagnetic spectrum and underpin some of the most advanced measurements in physics [1,2]. Usually, they are derived from femtosecond pulsed lasers and their frequency components are described by  $\nu_m = m f_{\text{rep}} + f_{\text{ceo}}$ , where  $f_{\text{rep}}$  and  $f_{\text{ceo}}$  are the laser's pulse repetition rate and carrier-envelope-offset frequency, and  $m \in \mathbb{N}_0$  is the comb line index. While the initial comb spectra are often limited in span by the laser gain medium, nonlinear spectral broadening through self-phase modulation (SPM) in optical fibers [3] has enabled octave spanning spectra [4], which are now routinely used to implement self-referencing, i.e., detection of  $f_{\text{ceo}}$  as a beating between harmonics of the comb [5–8]. Complementing silica fibers and specialty fibers [9], waveguides are efficient nonlinear platforms, providing access not only to self-phase modulation (SPM) but also to second-order nonlinear processes such as sum-frequency generation (SFG) and difference-frequency generation (DFG) [10]. Especially in nanophotonic waveguides [11],

effects beyond SPM have enabled ultrabroadband spectra and power efficient implementation of  $f_{\text{ceo}}$  beat note detection [12–24], holding potential for optical spectroscopy and efficient phase-coherent links from infrared to ultraviolet wavelengths. Generally, in multi-octave spectra, the broadened fundamental comb can overlap with its harmonics that can result from e.g., concurrent SFG and DFG. This implies that, where different harmonics overlap, combs with different offset frequencies are interleaved and the equidistance of the frequency comb modes is broken.

Here, we study the nonlinear spectral dynamics in the generation of broadband comb spectra where an overlap between different harmonics occurs. Strikingly, we find that the interleaved combs do not remain confined to the narrow spectral band where harmonics initially overlap, but that they can extend across the entire spectrum. This can give rise to an entire set of multiple broadband mutually offset interleaved combs. Their mutual offsets can be minimized, in the special case where the pump laser is arranged to be offset-free ( $f_{\text{ceo}} = 0$ ). These findings are of immediate relevance to comb-based techniques that seek to leverage multi-octave spectra as those accessible in photonic-integrated waveguides.

Figure 1 illustrates the spectral evolution and formation of a broadband spectrum during propagation in a nonresonant waveguide with second- and third-order nonlinearity, driven by a femtosecond mode-locked laser; similar reasoning will also apply to a purely third-order nonlinear waveguide with third-harmonic (triple-sum-frequency) generation: SPM broadens the input spectrum and the second-order nonlinearity creates SFG and DFG spectra. If the broadening is sufficiently strong, the input comb with

\*Contact author: tobias.herr@desy.de

†Present address: Université du Luxembourg, L-1511 Luxembourg, Luxembourg.

‡Present address: Swiss Center for Electronics and Microtechnology (CSEM), 2000 Neuchâtel, Switzerland.

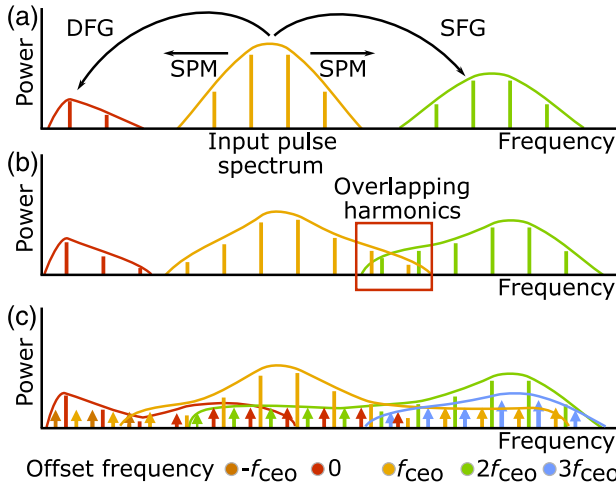


FIG. 1. Spectral dynamics in broadband frequency combs with overlapping harmonics generated by pumping nonresonant chip-integrated waveguides with femtosecond mode-locked lasers. (a) Self-phase modulation (SPM), as well as sum frequency generation (SFG) and difference frequency generation (DFG) result in spectral broadening and harmonic generation. (b) As the spectrum evolves, harmonics may overlap. (c) Harmonics with different offsets enter into additional nonlinear mixing processes, resulting in nonlinear gain for combs at new offset frequencies throughout the spectrum.

offset frequency  $f_{\text{ceo}}$ , the SFG spectrum with offset frequency  $2f_{\text{ceo}}$ , and the DFG spectrum with zero offset may start overlapping. In the overlapping spectral intervals this will result in interleaved combs with the same repetition rate  $f_{\text{rep}}$  but with different offsets. As in this case the nonlinear gain window of different nonlinear processes overlap, there will be additional nonlinear mixing dynamics between combs that can in principle extend the interleaved combs across the entire spectrum, similar to related dynamics observed in microresonators with third-order nonlinearity [25–27]. This could even result in the generation of additional interleaved combs with offsets corresponding to integer multiples of  $f_{\text{ceo}}$ . An experimental signature indicating the presence of broadband interleaved combs would be the detection of the offset frequency beat note  $f_{\text{ceo}}$  in narrow spectral intervals across the entire spectrum, particularly outside the narrow spectral interval where the harmonics initially overlap. If multiple interleaved combs are present at the same spectral position, additional beat notes between combs with offsets of integer multiples of  $f_{\text{ceo}}$  are expected.

*Comb line resolved simulations*—To understand the nonlinear spectral dynamics in realistic waveguides, we perform numerical simulations [28] based on the approach introduced in [29]. Specifically, we simulate a lithium niobate waveguide with a cross section of  $1000 \text{ nm} \times 800 \text{ nm}$  and sidewall angle of  $75^\circ$ . Its group-velocity dispersion is derived via finite element methods using the extraordinary refractive index of  $\text{LiNbO}_3$  from [30] and

the refractive index of  $\text{SiO}_2$  from [31]. The second-order nonlinearity  $d_{33}$  is set to  $31 \text{ pm/V}$  and the nonlinear refractive index  $n_2$  is set to  $2.65 \times 10^{-19} \text{ m}^2 \text{ W}^{-1}$  [32]. The waveguide length is 5 mm of which the last third is periodically poled with a chirped poling period  $\Lambda(z)$  ranging from 1 to  $15 \mu\text{m}$  and 50% duty cycle, to achieve broadband quasi-phase matching. To spectrally resolve comb lines belonging to interleaved combs with different offsets, we use a periodic simulation time window that includes 32 sech<sup>2</sup>-shaped input pulses with 120 pJ pulse energy, carrier frequency of 200 THz, 50 fs duration, and a periodicity of  $f_{\text{rep}}^{-1} = 375 \text{ ps}$ , sufficiently long to avoid temporal overlap between consecutive pulses during propagation [see Supplemental Material (SM), Sec. S1 for more details on the simulation [33]]. We define the input pulse train with  $f_{\text{ceo}} = f_{\text{rep}}/4$ , so that interleaved combs with offsets 0,  $f_{\text{ceo}}$ ,  $2f_{\text{ceo}}$ , and  $3f_{\text{ceo}}$  can be distinguished. Overall, the spectrum may contain frequencies  $\nu_{m,n} = mf_{\text{rep}} + nf_{\text{ceo}}$ , with the harmonic index  $n \in \mathbb{N}_0$  ( $n = 1$  for the input pulse).

From the simulated nonlinear dynamics, we extract the spectral envelope of each harmonic  $n$  along the spatial propagation coordinate  $z$  as shown in Fig. 2(a). The input spectrum ( $n = 1$ ) broadens and initially well separated second ( $n = 2$ ) and third ( $n = 3$ ) harmonic spectra are generated, which then start to overlap. During continued propagation, including in the periodically poled portion of the waveguides, the harmonics spread throughout the entire spectrum, forming effectively a set of multiple interleaved broadband combs with different  $n$ . The upper panels of Fig. 2(b) show the spectra in a narrow spectral window around 75 and 200 THz, where the resolved interleaved combs are visible. In contrast, if the pulse train is defined to have  $f_{\text{ceo}} = 0$ , interleaved combs are absent as can be seen in the lower panels of Fig. 2(b) showing the same spectral windows.

*Experiments*—To support our findings experimentally, we use a 5 mm long  $x$ -cut LNOI waveguide with  $\text{SiO}_2$  cladding that is pumped in the fundamental TE mode (polarization parallel to the optical axis of  $\text{LiNbO}_3$ ). The waveguide has a cross section of  $2300 \text{ nm} \times 800 \text{ nm}$ , and the last 1.5 mm (excluding the output coupling taper) of the waveguide is periodically poled with a chirped poling period as in the simulation. Detailed waveguide fabrication methods can be found in a previous Letter [34]. The experimental setup is shown in Fig. 3(a), where the pump laser is a sub-100 fs mode-locked laser with a center wavelength of 1560 nm and a repetition rate of 100 MHz. The light is coupled into and out of the waveguides via lensed fibers, and all fiber components are polarization maintaining and single mode at 1560 nm. The coupling efficiency is approximately 23% per facet and the on-chip pulse energy is varied from 139 to 347 pJ. Optical spectrum analyzers (OSAs) are used to record the broadband output spectra. As the resolution of our OSAs is insufficient to

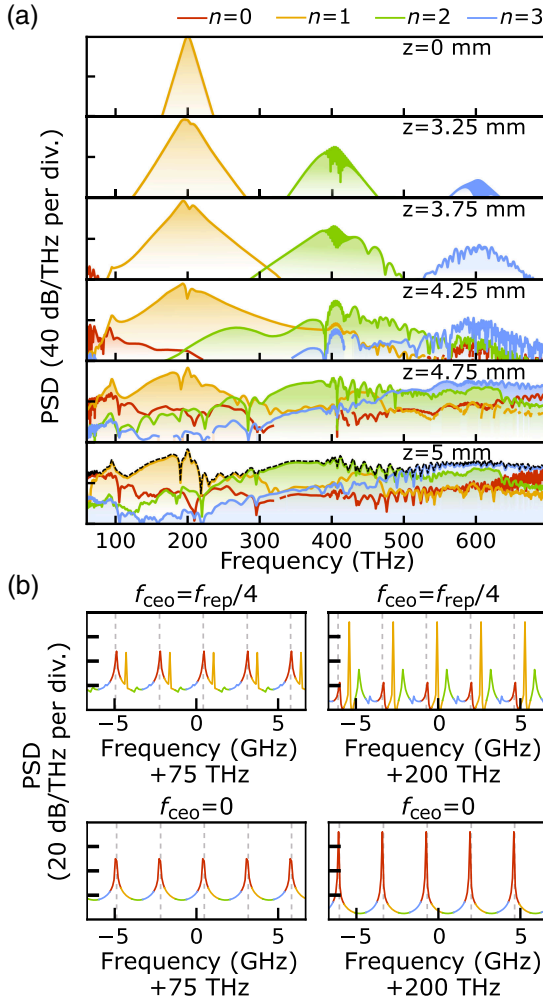


FIG. 2. Numerical simulation results. (a) Power spectral density (PSD) envelope of each harmonic indexed by  $n$  along the propagation coordinate  $z$  ( $n = 0$ , red;  $n = 1$ , orange;  $n = 2$ , green;  $n = 3$ , blue). The black dashed line in the bottom panel indicates the total PSD envelope with all harmonics combined. (b) PSD obtained from comb-line resolving simulation plotted with high resolution around frequencies of 75 and 200 THz. The upper two panels are for  $f_{\text{ceo}} = f_{\text{rep}}/4$ , the lower two panels for  $f_{\text{ceo}} = 0$ . Dashed gray lines mark an offset-free,  $f_{\text{rep}}$ -spaced grid. To better distinguish different harmonics, as a guide to the eye, the PSD has been color coded as in (a). Additional high-resolution plots are presented in Fig. S2 in SM [33].

resolve individual comb lines, we perform radio-frequency (rf) beat note measurements. For these measurements, the light is collimated to free space via an off-axis parabolic mirror, and a long-pass dichroic mirror (DM) splits the light with transmission wavelength starting from 950 nm to avoid potential ambiguity. Then the light is sent through bandpass filters (BPFs) before reaching the photodetectors (PDs). A neutral density filter (ND) is placed in the long wavelength optical path to avoid saturating the PD. The generated rf signals are measured by an electrical spectrum analyzer (ESA).

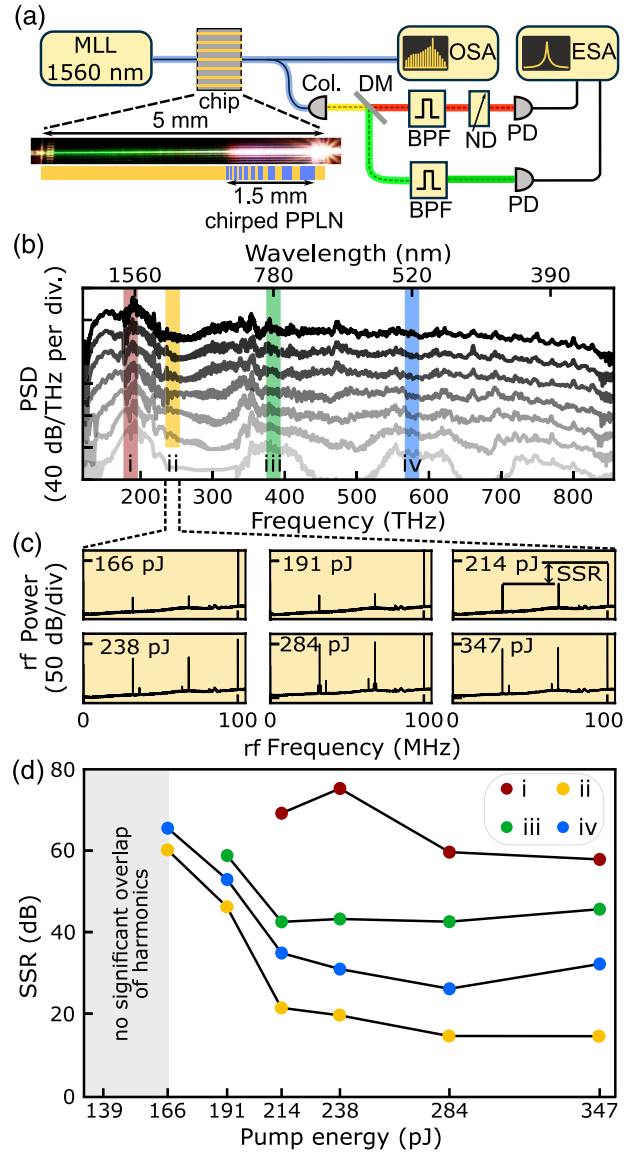


FIG. 3. Experiments with nonzero offset. (a) Schematic setup and a photograph of the chip during operation. PPLN, periodically poled lithium niobate; OSA, optical spectrum analyzer; ESA, electrical spectrum analyzer; Col., collimator; DM, dichroic mirror; BPF, bandpass filter; ND, neutral density filter; PD, photodetector. (b) Optical spectra with increasing pump energy (faded to dark: 139 pJ, 166 pJ, 191 pJ, 214 pJ, 238 pJ, 284 pJ, and 347 pJ). The spectra are shifted by 25 dB for visibility. Colored vertical bars mark frequency positions used to measure the rf beat note, with (i)  $1610 \pm 6$  nm, (ii)  $1300 \pm 15$  nm, (iii)  $780 \pm 5$  nm, and (iv)  $520 \pm 18$  nm. (c) The rf beat note at around 1300 nm with increasing pump energy with resolution bandwidth (RBW) of 10 kHz. (d) Scaling of the sideband suppression ratio (SSR) with the pulse energy. Data points represent the ratio between  $P_{\text{rep}}$  and  $P_{\text{ceo}}$  at different frequencies marked in (b).

Figure 3(b) shows the output spectra observed for different pump pulse energies, similar to the spectral evolution with increasing propagation distance in the simulation. For the lowest pulse energy, the harmonics

are well separated, but with increasing pulse energy merge into a gap-free spectrum spanning from mid-infrared to ultraviolet wavelengths. The rf signals are measured around the fundamental pump wavelength, its second harmonic and third harmonic, as well as around 1300 nm, as indicated by the color bands in Fig. 3(b). For the lowest pulse energy of 139 pJ, where harmonics are well separated, no  $f_{\text{ceo}}$  signal is observed in any wavelength band, despite the rf power of  $f_{\text{rep}}$  in the bands within the second and third harmonic regions exceeding the PD noise floor by more than 60 dB (see Fig. S3 in SM [33]). This changes with increasing pulse energy, as shown in Fig. 3(c) for the  $1300 \pm 15$  nm band and in SM (Fig. S3) [33] for other wavelength bands: as the harmonic gaps close, an  $f_{\text{ceo}}$  signal emerges at 166 pJ pulse energy, marked by two rf peaks between 0 and  $f_{\text{rep}} = 100$  MHz, indicating the formation of interleaved combs. (We validate this interpretation through high-resolution heterodyne continuous-wave laser spectroscopy, SM, Fig. S5 [33].) For higher pulse energy the strength of the  $f_{\text{ceo}}$  signal increases and two additional offset beat notes appear for a pulse energy above 238 pJ, indicating the simultaneous presence of at least three interleaved combs at 1300 nm.

The power level of the repetition rate and the offset frequency beat notes from the interleaved combs may be used to estimate the relative power levels of the interleaved comb lines. To simplify this estimation, we assume that only two interleaved combs  $n = i, j$  are present (i.e., any additional interleaved combs are of much less power) and that the spectral envelope and phase of the lines within each of the interleaved combs does not vary significantly across the bandwidth of the filter: denoting with  $A_{m,n}$  the (complex) field strength of the comb line with frequency  $\nu_{m,n}$ , the rf power levels in the repetition rate beat note and the offset frequency beat notes are

$$P_{\text{rep}} = \eta(|A_{m,i}A_{m-1,i}^*|^2 + |A_{m,j}A_{m-1,j}^*|^2) \approx \eta(P_{m,i}^2 + P_{m,j}^2), \quad (1)$$

$$P_{\text{ceo}} = \eta(|A_{m,i}A_{m,j}^*|^2 + |A_{m-1,i}A_{m-1,j}^*|^2) \approx 2\eta P_{m,i} P_{m,j}, \quad (2)$$

where lines with  $m$  and  $m - 1$  are assumed to pass through the spectral filter, and  $\eta$  is a constant that depends on the filter bandwidth and the detection efficiency. Assuming the interleaved comb with  $n = i$  is significantly more powerful than the one with  $n = j$ , we define the sideband suppression ratio (SSR) of the dominant comb as the power ratio between the two combs:

$$\text{SSR} := \frac{P_{m,i}}{P_{m,j}} \approx \frac{2P_{\text{rep}}}{P_{\text{ceo}}}, \quad (3)$$

where in the experiment the SSR is limited by the rf noise floor which defines a minimum value of  $P_{\text{ceo}}$ . Figure 3(d)

shows the SSR obtained through this estimation for the different wavelength bands. The SSR drastically drops for very broadband spectra and may be as low as 15 dB at 1300 nm. Such low SSR (low power contrast) may become problematic for some applications like dual-comb spectroscopy [35,36], spectroscopy based on individual comb line detection [37] or astronomical spectrograph calibration [38,39]. However, as the coherence of the comb lines is preserved (at least in the filtered frequency bands where narrow  $f_{\text{rep}}$  and  $f_{\text{ceo}}$  beat notes are observed), phase-coherent links across the comb spectrum may still be implemented if the interleaved comb line spectrum is accounted for.

The simulation suggests that a single, equidistant frequency comb can be generated when the pump source is arranged with  $f_{\text{ceo}} = 0$ . To explore this experimentally, we pump the waveguides with an amplified offset-free femtosecond source based on a DFG (TOPTICA DFC CORE 200+) [40], providing 472 pJ pulse energy (on-chip) at a center wavelength of 1560 nm with 59 fs pulse duration at 200 MHz repetition rate and aligned in TE polarization. For this laser, it has been demonstrated that the performance is statistically consistent with  $f_{\text{ceo}} = 0$  down to the few- $\mu$ Hz level [41]. The waveguide has the same parameters as the one in the aforementioned experiments, except the cross section is 1800 nm  $\times$  800 nm which results in the broadest spectrum at this pump configuration [Fig. 4(a)]. Indeed, the rf measurements do not show an offset signal in any of the filter bands [Fig. 4(b)]; also see higher resolution recordings of the rf beat notes presented in Fig. S4 in SM [33], consistent with a spectrum where the offsets between interleaved combs are minimized; a locking dynamics as observed in

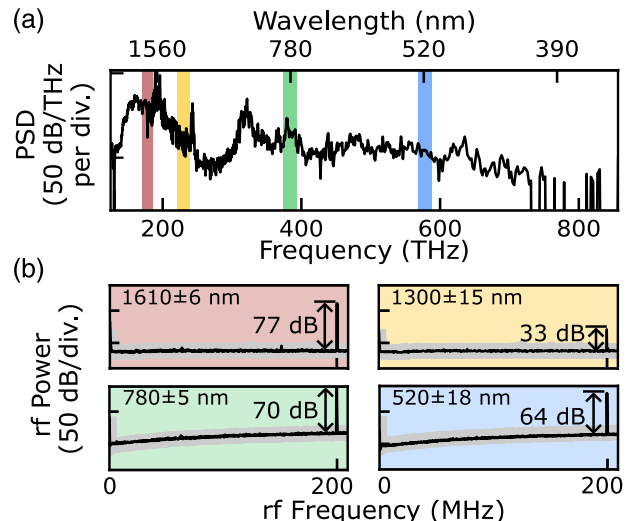


FIG. 4. Experimental results with offset-free pump source. (a) Generated optical spectrum. (b) rf beat note measured at optical frequencies same as in the non-offset-free pump experiments. Gray backgrounds mark the noise floor of measurements. RBW = 1 kHz.

microresonators [42] is absent here as the waveguide does not provide feedback to the laser.

**Conclusion**—Highly efficient nonlinear waveguides enable ultrabroadband frequency combs. Overlap between harmonics can occur in such spectra, leading to a set of interleaved combs with different offset frequencies and these interleaved combs can extend across the entire spectrum. While this effectively results in a nonequidistant spectrum of lines, the frequency components are still well defined and we do not observe a loss of coherence in the comb lines. Thus, if the interleaved combs are taken into account, these spectra are still suitable for coherent heterodyning with external lasers and phase-coherent links across the spectrum. When aiming at  $f_{\text{CEO}}$  detection, it is possible that the strongest signal may be obtained outside the spectral interval of initial harmonic overlap. For comb-based techniques that rely on the regularity of the comb spectrum and absence of interleaved lines, such as dual-comb spectroscopy, spectroscopy based on individual comb line detection, or astronomical spectrograph calibration, overlap between harmonics should be avoided. Alternatively, when the waveguide is pumped with an offset-free source [40,43], the offset between interleaved combs can be minimized, creating new opportunities for ultrabroadband optical precision measurements across multiple octaves.

**Acknowledgments**—This project has received funding from the European Research Council (ERC, Grant No. 853564), the European Innovation Council (EIC, Grant No. 101046920), the Swiss National Science Foundation (Sinergia, Grant No. 00020\_182598), and through the Helmholtz Young Investigators Group VH-NG-1404. The fabrication of the lithium niobate waveguides was carried out at the Center for Micro-NanoTechnology (CMi) at EPFL, and simulations were supported through the Maxwell computational resources operated at DESY.

**Data availability**—The data that support the findings of this Letter are available [44].

- [1] T. Fortier and E. Baumann, 20 years of developments in optical frequency comb technology and applications, *Commun. Phys.* **2**, 1 (2019).
- [2] S. A. Diddams, K. Vahala, and T. Udem, Optical frequency combs: Coherently uniting the electromagnetic spectrum, *Science* **369**, eaay3676 (2020).
- [3] J. M. Dudley, G. Genty, and S. Coen, Supercontinuum generation in photonic crystal fiber, *Rev. Mod. Phys.* **78**, 1135 (2006).
- [4] J. K. Ranka, R. S. Windeler, and A. J. Stentz, Visible continuum generation in air–silica microstructure optical fibers with anomalous dispersion at 800 nm, *Opt. Lett.* **25**, 25 (2000).
- [5] H. Telle, G. Steinmeyer, A. Dunlop, J. Stenger, D. Sutter, and U. Keller, Carrier-envelope offset phase control: A novel concept for absolute optical frequency measurement and ultrashort pulse generation, *Appl. Phys. B* **69**, 327 (1999).
- [6] R. Holzwarth, Th. Udem, T. W. Hänsch, J. C. Knight, W. J. Wadsworth, and P. St. J. Russell, Optical frequency synthesizer for precision spectroscopy, *Phys. Rev. Lett.* **85**, 2264 (2000).
- [7] D. J. Jones, S. A. Diddams, J. K. Ranka, A. Stentz, R. S. Windeler, J. L. Hall, and S. T. Cundiff, Carrier-envelope phase control of femtosecond mode-locked lasers and direct optical frequency synthesis, *Science* **288**, 635 (2000).
- [8] T. Udem, R. Holzwarth, and T. W. Hänsch, Optical frequency metrology, *Nature (London)* **416**, 233 (2002).
- [9] T. Sylvestre, E. Genier, A. N. Ghosh, P. Bowen, G. Genty, J. Troles, A. Mussot, A. C. Peacock, M. Klimczak, A. M. Heidt, J. C. Travers, O. Bang, and J. M. Dudley, Recent advances in supercontinuum generation in specialty optical fibers [Invited], *J. Opt. Soc. Am. B* **38**, F90 (2021).
- [10] C. Langrock, M. M. Fejer, I. Hartl, and M. E. Fermann, Generation of octave-spanning spectra inside reverse-proton-exchanged periodically poled lithium niobate waveguides, *Opt. Lett.* **32**, 2478 (2007).
- [11] C.-S. Brès, A. D. Torre, D. Grassani, V. Brasch, C. Grillet, and C. Monat, Supercontinuum in integrated photonics: Generation, applications, challenges, and perspectives, *Nanophotonics* **12**, 1199 (2023).
- [12] D. D. Hickstein, H. Jung, D. R. Carlson, A. Lind, I. Coddington, K. Srinivasan, G. G. Ycas, D. C. Cole, A. Kowlig, C. Fredrick, S. Droste, E. S. Lamb, N. R. Newbury, H. X. Tang, S. A. Diddams, and S. B. Papp, Ultrabroadband supercontinuum generation and frequency-comb stabilization using on-chip waveguides with both cubic and quadratic nonlinearities, *Phys. Rev. Appl.* **8**, 014025 (2017).
- [13] D. R. Carlson, D. D. Hickstein, A. Lind, S. Droste, D. Westly, N. Nader, I. Coddington, N. R. Newbury, K. Srinivasan, S. A. Diddams, and S. B. Papp, Self-referenced frequency combs using high-efficiency silicon-nitride waveguides, *Opt. Lett.* **42**, 2314 (2017).
- [14] Y. Okawachi, M. Yu, J. Cardenas, X. Ji, A. Klenner, M. Lipson, and A. L. Gaeta, Carrier envelope offset detection via simultaneous supercontinuum and second-harmonic generation in a silicon nitride waveguide, *Opt. Lett.* **43**, 4627 (2018).
- [15] D. D. Hickstein, D. R. Carlson, H. Mundoor, J. B. Khurgin, K. Srinivasan, D. Westly, A. Kowlig, I. I. Smalyukh, S. A. Diddams, and S. B. Papp, Self-organized nonlinear gratings for ultrafast nanophotonics, *Nat. Photonics* **13**, 494 (2019).
- [16] M. Yu, B. Desiatov, Y. Okawachi, A. L. Gaeta, and M. Lončar, Coherent two-octave-spanning supercontinuum generation in lithium-niobate waveguides, *Opt. Lett.* **44**, 1222 (2019).
- [17] E. Obrzud, V. Brasch, T. Voumard, A. Stroganov, M. Geiselmann, F. Wildi, F. Pepe, S. Lecomte, and T. Herr, Visible blue-to-red 10 GHz frequency comb via on-chip triple-sum-frequency generation, *Opt. Lett.* **44**, 5290 (2019).
- [18] Y. Okawachi, M. Yu, B. Desiatov, B. Y. Kim, T. Hansson, M. Lončar, and A. L. Gaeta, Chip-based self-referencing

using integrated lithium niobate waveguides, *Optica* **7**, 702 (2020).

[19] J. Lu, X. Liu, A. W. Bruch, L. Zhang, J. Wang, J. Yan, and H. X. Tang, Ultraviolet to mid-infrared supercontinuum generation in single-crystalline aluminum nitride waveguides, *Opt. Lett.* **45**, 4499 (2020).

[20] E. Obrzud, S. Denis, H. Sattari, G. Choong, S. Kundermann, O. Dubochet, M. Despont, S. Lecomte, A. H. Ghadimi, and V. Brasch, Stable and compact RF-to-optical link using lithium niobate on insulator waveguides, *APL Photonics* **6**, 121303 (2021).

[21] D. M. B. Lesko, H. Timmers, S. Xing, A. Kowligly, A. J. Lind, and S. A. Diddams, A six-octave optical frequency comb from a scalable few-cycle erbium fibre laser, *Nat. Photonics* **15**, 281 (2021).

[22] T.-H. Wu, L. Ledezma, C. Fredrick, P. Sekhar, R. Sekine, Q. Guo, R. M. Briggs, A. Marandi, and S. A. Diddams, Visible-to-ultraviolet frequency comb generation in lithium niobate nanophotonic waveguides, *Nat. Photonics* **18**, 218 (2024).

[23] M. Ludwig, F. Ayhan, T. M. Schmidt, T. Wildi, T. Voumard, R. Blum, Z. Ye, F. Lei, F. Wildi, F. Pepe, M. A. Gaafar, E. Obrzud, D. Grassani, O. Hefti, S. Karlen, S. Lecomte, F. Moreau, B. Chazelas, R. Sottile, V. Torres-Company, V. Brasch, L. G. Villanueva, F. Bouchy, and T. Herr, Ultraviolet astronomical spectrograph calibration with laser frequency combs from nanophotonic lithium niobate waveguides, *Nat. Commun.* **15**, 7614 (2024).

[24] W. Fan, M. Ludwig, I. Rousseau, I. Arabadzhiev, B. Ruhnke, T. Wildi, and T. Herr, Supercontinua from integrated gallium nitride waveguides, *Optica* **11**, 1175 (2024).

[25] T. Herr, K. Hartinger, J. Riemensberger, C. Y. Wang, E. Gavartin, R. Holzwarth, M. L. Gorodetsky, and T. J. Kippenberg, Universal formation dynamics and noise of Kerr-frequency combs in microresonators, *Nat. Photonics* **6**, 480 (2012).

[26] C. J. Flower, M. Jalali Mehrabad, L. Xu, G. Moille, D. G. Suarez-Forero, O. Örsel, G. Bahl, Y. Chembo, K. Srinivasan, S. Mittal, and M. Hafezi, Observation of topological frequency combs, *Science* **384**, 1356 (2024).

[27] T. P. Letsou, D. Kazakov, P. Ratra, L. L. Columbo, M. Brambilla, F. Prati, C. Rimoldi, S. Dal Cin, N. Opačak, H. O. Everitt, M. Piccardo, B. Schwarz, and F. Capasso, Hybridized soliton lasing in coupled semiconductor lasers, *Phys. Rev. Lett.* **134**, 023802 (2025).

[28] T. Voumard, M. Ludwig, T. Wildi, F. Ayhan, V. Brasch, L. G. Villanueva, and T. Herr, Simulating supercontinua from mixed and cascaded nonlinearities, *APL Photonics* **8**, 036114 (2023).

[29] M. Conforti, A. Marini, T. X. Tran, D. Faccio, and F. Biancalana, Interaction between optical fields and their conjugates in nonlinear media, *Opt. Express* **21**, 31239 (2013).

[30] D. E. Zelmon, D. L. Small, and D. Jundt, Infrared corrected Sellmeier coefficients for congruently grown lithium niobate and 5 mol.% magnesium oxide-doped lithium niobate, *J. Opt. Soc. Am. B* **14**, 3319 (1997).

[31] I. H. Malitson, Interspecimen comparison of the refractive index of fused silica, *J. Opt. Soc. Am.* **55**, 1205 (1965).

[32] C. R. Phillips, C. Langrock, J. S. Pelc, M. M. Fejer, I. Hartl, and M. E. Fermann, Supercontinuum generation in quasi-phasematched waveguides, *Opt. Express* **19**, 18754 (2011).

[33] See Supplemental Material at <http://link.aps.org/supplemental/10.1103/kgd7-52hy> for further details on the simulations, beat note measurements and comb line spectroscopy.

[34] F. Ayhan, M. Ludwig, T. Herr, V. Brasch, and L. G. Villanueva, Fabrication of periodically poled lithium niobate waveguides for broadband nonlinear photonics, *APL Photonics* **10**, 016118 (2025).

[35] I. Coddington, N. Newbury, and W. Swann, Dual-comb spectroscopy, *Optica* **3**, 414 (2016).

[36] N. Picqué and T. W. Hänsch, Frequency comb spectroscopy, *Nat. Photonics* **13**, 146 (2019).

[37] S. A. Diddams, L. Hollberg, and V. Mbele, Molecular fingerprinting with the resolved modes of a femtosecond laser frequency comb, *Nature (London)* **445**, 627 (2007).

[38] T. Herr and R. A. McCracken, Astrocombs: Recent advances, *IEEE Photonics Technol. Lett.* **31**, 1890 (2019).

[39] N. Jovanovic *et al.*, 2023 Astrophotonics Roadmap: Pathways to realizing multi-functional integrated astrophotonic instruments, *J. Phys. Photonics* **5**, 042501 (2023).

[40] G. Krauss, D. Fehrenbacher, D. Brida, C. Riek, A. Sell, R. Huber, and A. Leitenstorfer, All-passive phase locking of a compact Er: Fiber laser system, *Opt. Lett.* **36**, 540 (2011).

[41] H. Tian, T. Liao, M. Volkov, T. Puppe, K. Predehl, B. Lu, Z. Fang, Y. Lin, and G. Steinmeyer, Critical thermal drifts in external fiber amplifiers limit optical frequency metrology, *Opt. Lett.* **50**, 6313 (2025).

[42] T. Wildi, A. Ulanov, N. Englebert, T. Voumard, and T. Herr, Sideband injection locking in microresonator frequency combs, *APL Photonics* **8**, 120801 (2023).

[43] S. Okubo, A. Onae, K. Nakamura, T. Udem, and H. Inaba, Offset-free optical frequency comb self-referencing with an f-2f interferometer, *Optica* **5**, 188 (2018).

[44] W. Fan, F. Ayhan, T. Wildi, M. Volkov, A. Seer, M. Ludwig, T. Voumard, A. Brodschelm, V. Brasch, G. L. Villanueva, and T. Herr, Supporting data “Spectral dynamics in broadband frequency combs with overlapping harmonics”, v1, zenodo, [10.5281/zenodo.14999180](https://doi.org/10.5281/zenodo.14999180) (2025).